Sensors and Materials, Vol. 34, No. 4 (2022) 1561–1575
MYU Tokyo

S & M 2910

Multifunctional Implantable Device for Simultaneous Optical and Electrophysiological Measurements

Kyosuke Naganuma,[1] Yasumi Ohta,[1] Takaaki E. Murakami,[1] Ryoma Okada,[1]
Mark Christian Guinto,[1] Hironari Takehara,[1] Makito Haruta,[1]
Hiroyuki Tashiro,[1,2] Kiyotaka Sasagawa,[1] Yoshinori Sunaga,[3]
Yasemin M. Akay,[3] Metin Akay,[3] and Jun Ohta[1*]

[1]Division of Materials Science, Graduate School of Science and Technology,
Nara Institute of Science and Technology, 8916-5 Ikoma, Nara 630-0192, Japan
[2]Division of Medical Technology, Department of Health Sciences, Faculty of Medical Sciences, Kyushu University,
3-1-1 Maidashi, Higashi-ku, Fukuoka 812-8582, Japan
[3]Department of Biomedical Engineering, University of Houston, Houston, TX 77204, USA

(Received October 18, 2021; accepted February 21, 2022)

Keywords: implantable device, electrophysiology, fluorescence imaging, multifunctional device, *in vivo* experiment

In neuroscience, it is crucial to clarify the relationship between single-cell activity and neural network structure to understand brain neural activity. To this end, a device that can measure signals with high temporal resolution over a wide area is required. In this study, we developed a multifunctional implantable device for measuring deep-brain functions. The device conducts electrophysiological measurements using microelectrodes and fluorescence imaging using a CMOS image sensor, which enables observations of brain functions with high temporal resolution over a wide area. The device developed is implemented by stacking the microelectrode array and imaging device. We measured the activity of neurons in the ventral tegmental area (VTA) of mice using this device. We successfully recorded action potentials and confirmed that the developed microelectrodes are effective for measuring brain functions. Results suggest that the multifunctional implantable device developed can simultaneously perform electrophysiological measurements and fluorescence imaging using a CMOS image sensor. However, the noise generated during imaging should be eliminated in the future. The activation of γ-aminobutyric acid neurons was also confirmed upon the intraperitoneal injection of nicotine solution as a pharmacological stimulus. The device developed with integrated microelectrodes and a CMOS image sensor is unprecedented and can prove useful in understanding the relationship between neuronal activity and neural networks.

1. Introduction

The mammalian brain, which is responsible for advanced information processing such as learning and cognition, is an extremely complex network consisting of millions to billions of

*Corresponding author: e-mail: ohta@ms.naist.jp
https://doi.org/10.18494/SAM3710

ISSN 0914-4935
https://myukk.org/

neurons.[1,2] Measuring the activity of the neurons that make up this network not only reveals the mechanisms of various information processing pathways but also enables the discovery of treatments for neurological diseases.[3] Therefore, the measurement of brain functions is very important from both neuroscientific and medical perspectives. However, to reveal unexplained brain functions, it is necessary to not only measure the activity of single cells but also understand the relationship between the activities of other cells in the vicinity at the neural-network level. Hence, it is necessary to develop a technique to simultaneously measure the activity of multiple neurons over a wide area.

The implantable imaging devices developed so far are equipped with CMOS image sensors, which enable lensless imaging with ultracompact and lightweight imaging devices without restricting the behavior of mice.[4–6] These devices are equipped with a micro-light-emitting diode (μ-LED) as the light source, which enables the excitation of fluorescent proteins, such as the genetically encoded calmodulin protein (GCaMP) for fluorescence imaging in close contact with the brain tissue and pixel array. In addition, by implanting multiple devices, it is possible to simultaneously investigate the mechanisms of various neural networks. The ability to observe the vertical plane makes it possible to observe neurons in directions that conventional imaging devices cannot capture. Moreover, deep-brain imaging has been demonstrated to be possible owing to the extremely small thickness of these devices and their minimal invasiveness.[7]

In this study, we aimed to simultaneously conduct electrophysiological measurements and fluorescence imaging to achieve high temporal resolution with wide-area observation. First, we independently developed a microelectrode array and a fluorescence imaging device. In addition to evaluating the performance of these devices, we demonstrated their functions through *in vivo* experiments in the ventral tegmental area (VTA) of mice. After functional verification, we integrated each device to construct a multifunctional implantable device with an unprecedented structure that enables both electrophysiological measurements using microelectrodes and fluorescence imaging via CMOS image sensors. Figure 1 shows the concept of this device. The multifunctional implantable device was implanted in the mouse VTA, and simultaneous electrophysiological measurements and fluorescence imaging were performed. In addition, a nicotine solution, which is known to activate γ-aminobutyric acid (GABA)-ergic and dopamine (DA)-ergic neurons, was intraperitoneally (IP) injected as a pharmacological stimulus.[8,9] Subsequently, the neuronal activity was recorded and compared with that before the injection. This device is expected to enable measurements that can be crucial in revealing the relationship between the activity of individual neurons and the structure of the neural network.

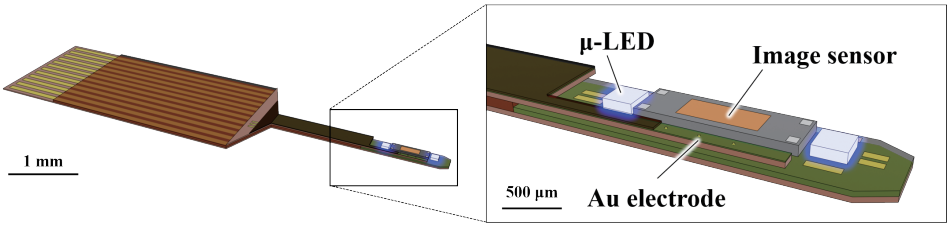

Fig. 1. (Color online) Concept of multifunctional implantable device.

2 Materials and Methods

2.1 Microelectrode array device

The microelectrode array device had three Au microelectrodes with a diameter of 20 μm at the tip and was formed with a custom-designed polyimide-based flexible printed circuit (FPC) (Taiyo Kogyo, Japan). The pitch of each microelectrode was 200 μm. This structure enables the observation of the electrical signals from neurons distributed in the mouse VTA. Figure 2(a) shows a photograph of the device, and Fig. 2(b) shows a scanning electron microscopy (SEM) image of the microelectrode. The thickness of the device was approximately 200 μm. In addition, polyimide was used as the substrate of the device. The Au microelectrodes were connected to a printed circuit board (PCB) by wire bonding with Cu wires and interconnected to the recording system using coaxial cables. In addition, the polyimide used in the microelectrode array device remained intact because the experiment was an acute one and its structure did not have the potential to cause tissue damage induced by electrical leakage. For long-term implantation in the future, the coating of the device with parylene-C is necessary for biocompatibility.

2.2 Electrochemical impedance spectroscopy

The signal-to-noise ratio (SNR) of extracellular potential recordings is affected by the thermal noise derived from the electrode impedance.[10,11] Figure 3 shows a diagram of the impedance measurement system. Measurements were performed in 0.1 M phosphate-buffered saline (PBS) (FUJIFILM Wako Pure Chemical Corporation, Japan). The working, reference, and counter electrodes were made of Au as the recording electrode on the device, Ag/AgCl (RE-1BP, ALS Co., Japan), and Pt, respectively. A sinusoidal wave of 10 mV_{pp} was input from a potentiostat (PGSTAT204, Metrohm Japan Ltd., Japan) equipped with a frequency response analyzer (FRA32M, Metrohm Japan Ltd., Japan). The frequency sweep range was set from 1 Hz to 100 kHz.

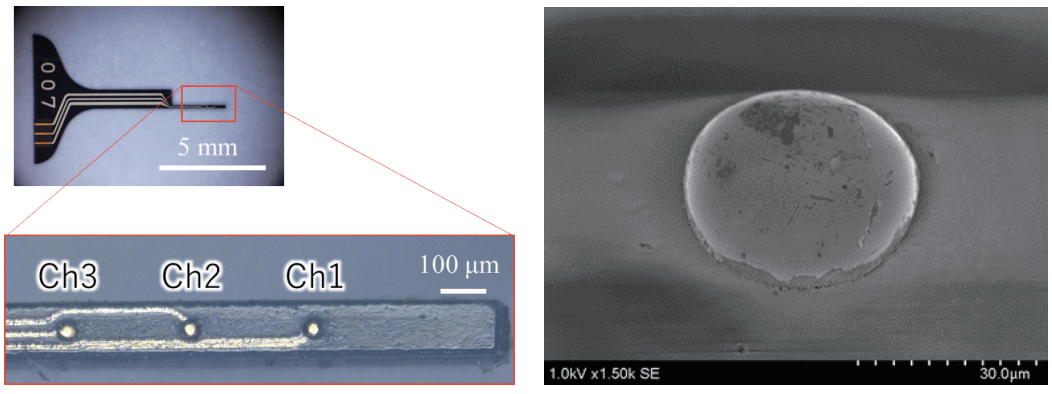

(a) (b)

Fig. 2. (Color online) Microelectrode array device. (a) Photograph of actual device. (b) SEM image of microelectrode.

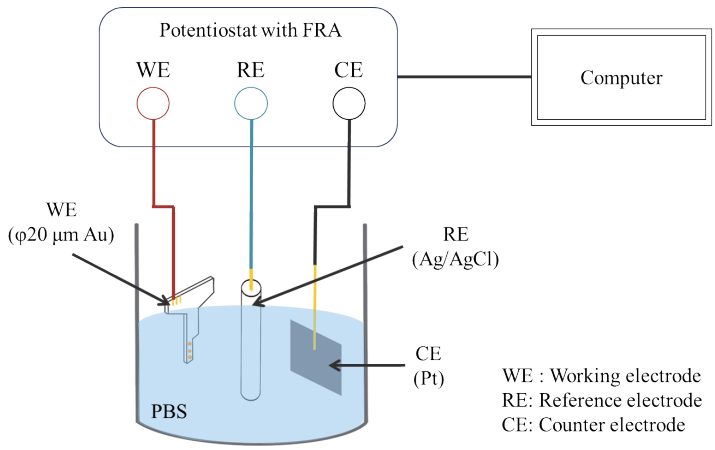

Fig. 3. (Color online) Experimental setup for electrochemical impedance spectroscopy.

2.3 Fluorescence imaging device with CMOS image sensor

The implantable imaging device used in this study was implemented by mounting a CMOS image sensor and LEDs on a FPC made of polyimide. A custom-made fluorescence filter was mounted on the image sensor to eliminate the excitation light from the LEDs. Furthermore, the entire device was coated with parylene-C to make it biocompatible and waterproof. The thickness of the parylene-C layer was approximately 5 μm. The CMOS image sensor used in the device was fabricated using a 0.35 μm standard CMOS process (0.35 μm, 2-poly-4-metal CMOS; TSMC, Taiwan). The pixel size was 7.5 × 7.5 μm^2, and the number of pixels was 40 × 120 (imaging area: 300 × 900 μm^2). The target area, VTA, had a width of approximately 500 μm in the depth direction. Thus, it can be assumed that brain neuronal activity in a sufficiently large area can be measured. Details of the image sensor specifications have been reported in a previous paper.[4] μ-LEDs (ES-CEBHM12A, EPISTAR Corp., Taiwan) with a central wavelength of 473 nm and a size of 350 × 280 μm^2 were installed as excitation light sources for fluorescent proteins. The FPC, CMOS image sensor, and μ-LEDs were connected by wire bonding. The fluorescence filter was made of UV-curable resin (NOA63, Norland Products, USA) as the base material and a mixture of a yellow dye (Valifast yellow 3150, Orient Chemical Industries Co., Ltd., Japan) and cyclopentanone (FUJIFILM Wako Pure Chemical Corporation, Japan).[7]

2.4 Device integration

The electrode array device was fixed on the side of the imaging device with epoxy resin to unify all devices. As a result, a structure with a recording electrode, image sensor, and μ-LED at the tip was fabricated. Figure 4(a) shows the device integration process, Fig. 4(b) shows a photograph of the integrated device, and Fig. 4(c) shows the SEM image of the tip of the device. We confirmed that the microelectrode of the device and the surface of the image sensor are of the same height.

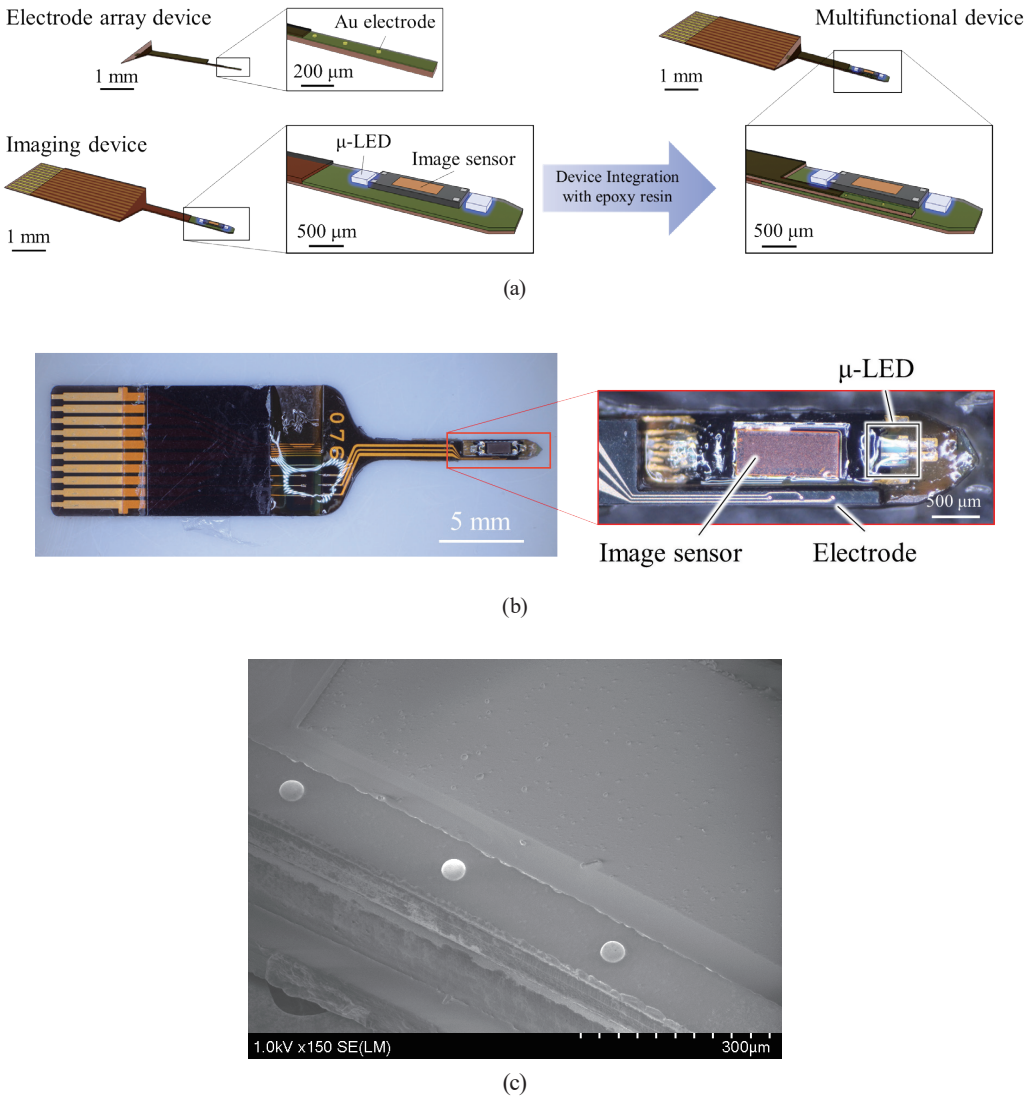

Fig. 4. (Color online) Multifunctional implantable device. (a) Device integration flow. (b) Photograph of actual device after integration. (c) SEM image of tip of device.

2.5 Surgery

All animal experiments were performed using protocols approved by the Nara Institute of Science and Technology (NAIST). All adult mice [C57BL6 (n = 9) for electrophysiological recording and Thy1-GCaMP6 (n = 3) for fluorescence imaging and simultaneous measurements] were kept on a 12 h light/12 h dark schedule. Access to standard food and water was provided *ad libitum*. The mice were mounted on a stereotaxic apparatus (Narishige, Japan) during surgery. All the animals were anesthetized with urethane before device implantation and during brain activity measurements.[12] The device was implanted through a small burr hole formed above the VTA [anteroposterior (AP) = −3.6 mm, mediolateral (ML) = ±0.4 mm] using a microdrill and a

manipulator. For the electrophysiological recordings, a microelectrode array device was implanted into the VTA [dorsoventral (*DV*) = 4.7–4.9 mm from the brain surface]. For fluorescence imaging and simultaneous measurements, the device developed was implanted into the VTA (*DV* = 5.8–6.0 mm from the brain surface).

2.6 *In vivo* experiment

For the electrophysiological measurements, a microelectrode array device attached to a manipulator (Narishige, Japan) was implanted. Saline solution was dripped into and around the hole at room temperature to prevent the brain tissue from drying out. Neuronal activity was measured by acute electrophysiological recordings using the implanted device. Spontaneous spikes (single- and multi-unit activities) were recorded at depths below *DV* = 4.7 mm. Subsequently, a nicotine [(–)-nicotine, Sigma-Aldrich, USA] solution (0.25 mg/kg) was IP injected and changes in elicited neuronal activity were recorded. The same amount of phosphate-buffered saline (PBS) as that of 0.25 mg/kg nicotine solution was IP injected as control. At this point, the reference electrode and ground (GND) used for measurement were common and connected to the ear bar, thus fixing the mouse head. The signals obtained from the mouse brain were input to a preamplifier (SH-MED8, Alpha MED Scientific Inc., Japan) with a 10-fold amplification factor and then connected to the main amplifier (SU-MED8, Alpha MED Scientific Inc., Japan) with a 100-fold amplification factor). The main amplifier was equipped with a 60 Hz notch filter and a 100–5000 Hz bandpass filter. The signals input to the main amplifier were recorded using Micro1401 mkII (Cambridge Electronic Design Ltd., UK) at a sampling frequency of 20 kHz/Ch and a resolution of 24 bits. The collected data were stored for offline analysis using MATLAB (MathWorks).

For GCaMP6 fluorescence imaging, an imaging device attached to a manipulator was implanted. After implantation, fluorescence was generated from GCaMPs by stimulating GABAergic neurons with excitation light emitted from a μ-LED light source. Fluorescence imaging was performed using a CMOS image sensor. Subsequently, a nicotine solution (0.25 mg/kg) was IP injected, and the change in fluorescence intensity was recorded. The measurements were performed at 10 frames per second (fps).

For simultaneous electrophysiological measurements and fluorescence imaging, a multifunctional device attached to a manipulator was implanted. After implantation, a nicotine solution (0.25 mg/kg) was IP injected and the changes in extracellular potential and fluorescence intensity before and after administration were compared. During simultaneous measurements, the clock signal used to drive the image sensor was detected by the electrodes as electromagnetic noise, which had a substantial effect on the electrophysiological measurements. To eliminate the effect of electromagnetic noise, fluorescence imaging was performed by driving the image sensor for approximately 10 s every 5 min after nicotine administration. Figure 5 shows a block diagram of the experimental setup for the simultaneous electrophysiological measurement and fluorescence imaging.

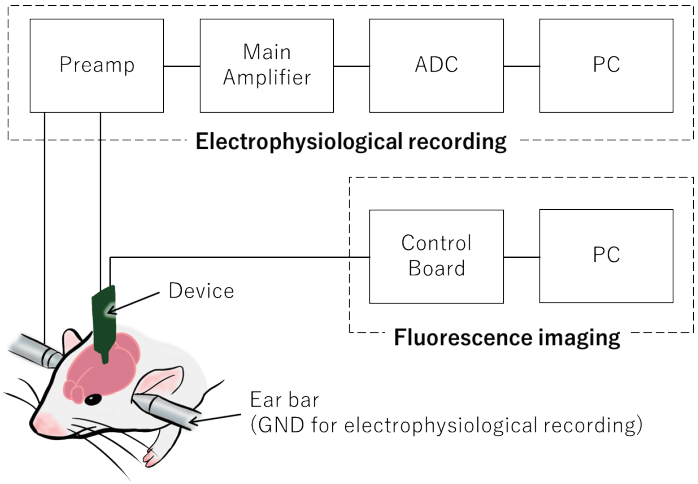

Fig. 5. (Color online) Experimental setup for simultaneous measurement.

2.7 Immunohistochemistry

Because the VTA contains numerous GABAergic and dopaminergic neurons, immunostaining was performed by the free-floating section method[13] using anti-c-Fos antibodies to examine the neurons stimulated by nicotine. Mice used for *in vivo* experiments were perfusion-fixed with saline and then 4% paraformaldehyde. After the perfusion fixation, the brains were extracted and immersed in 4% paraformaldehyde for 4 h, washed with PBS, and sliced into 40-μm-thick coronal slices using a vibratome (Linear Slicer PRO7, Dosaka). The slices were stained with mouse anti-c-Fos antibodies (Abcam, ab208942, 1:1000), which indicate neuronal activation, rabbit anti-tyrosine hydroxylase (TH) antibodies (Sigma-Aldrich, AB152, 1:1000), which label dopaminergic neurons, and rabbit anti-vesicular GABA transporter (VGAT) antibodies (Sigma-Aldrich, AB5062P, 1:100), which label GABAergic neurons. The secondary antibodies used were goat anti-mouse IgG Alexa Fluor 488 (Abcam, ab150113, 1:800) and goat anti-rabbit IgG Alexa Fluor 568 (Abcam, ab175471, 1:800).

3. Results and Discussion

Figure 6 shows the measured electrode impedance of the microelectrode array device. To obtain a high-quality recording, an impedance of less than 1 MΩ at 1 kHz, which is the frequency band of the action potential, is required to reduce thermal noise.[10,13] An electrode impedance of approximately 180 ± 12.7 kΩ (mean ± S.D.) (n = 9) was measured at 1 kHz. Therefore, the device developed in this study was confirmed to be suitable for extracellular recordings.

The obtained signals were analyzed using MATLAB, and results are presented here. The potentials obtained by extracellular recordings were divided into the local field potential (LFP) (0.1–300 Hz) and spike components (300–5000 Hz) according to the frequency.[14,15] Therefore, to isolate the spike components, we filtered the data using a 300 Hz high-pass filter. Figure 7(a)

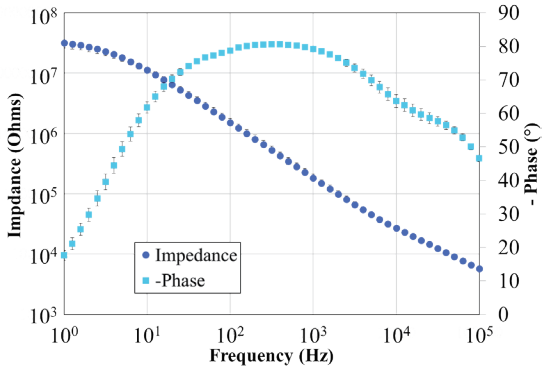

Fig. 6. (Color online) Electrode impedance.

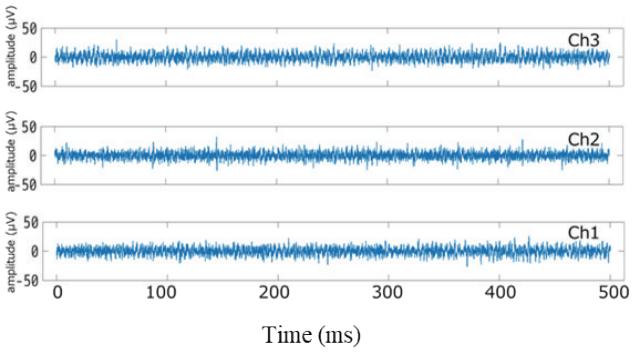

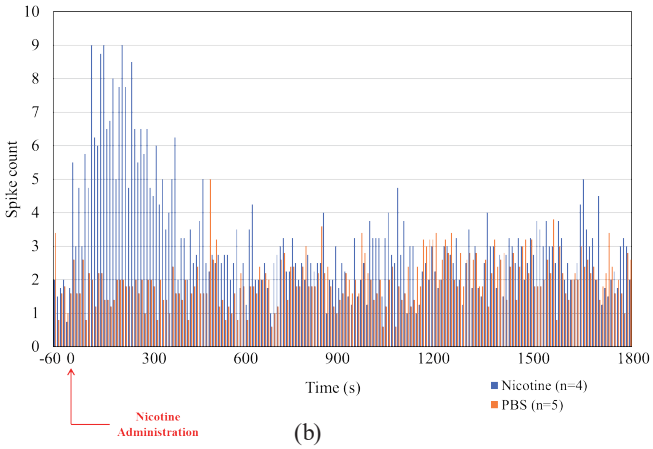

Fig. 7. (Color online) Results of electrophysiological measurements. (a) Waveforms of extracellular recordings of a spontaneously firing neuron. (b) Histogram of firing frequencies obtained before and after administration.

shows the waveforms of the extracellular recordings of a spontaneously firing neuron. Figure 7(b) shows a histogram of the firing frequencies obtained before and after nicotine (0.25 mg/kg) stimulation and PBS administration. The size of each bin in the histogram is 10 s. We found that the firing frequency started to increase approximately 1 min after nicotine administration. This

result is consistent with that of a previous study: the firing frequency begins to increase within 2 min after nicotine administration.[8] When the PBS was IP injected as control, the firing frequency was almost unchanged before and after administration unlike in the case of nicotine administration.

In the fluorescence imaging experiment, we measured the change in the fluorescence intensity of the neurons in the VTA. The reference fluorescence intensity before the stimulation was set as F_0, and the change in fluorescence intensity after the stimulation was set as ΔF. We measured the fluorescence intensity ratio $\Delta F/F_0$ in the region of interest (ROI) using the image sensor. Figures 8(a) and 8(b) show the changes in fluorescence intensity ratio during nicotine and PBS administration, respectively. In both the ROI measurements, $\Delta F/F_0$ increased after nicotine administration, suggesting that nicotine administration induced neuronal activity. In contrast, in the PBS administration experiment, $\Delta F/F_0$ was almost unchanged in all the ROIs. These results are consistent with those of a previous study.[7]

Finally, we describe the results of the simultaneous electrophysiological measurements and fluorescence imaging. Figure 9 shows the results of those simultaneous measurements. The bin

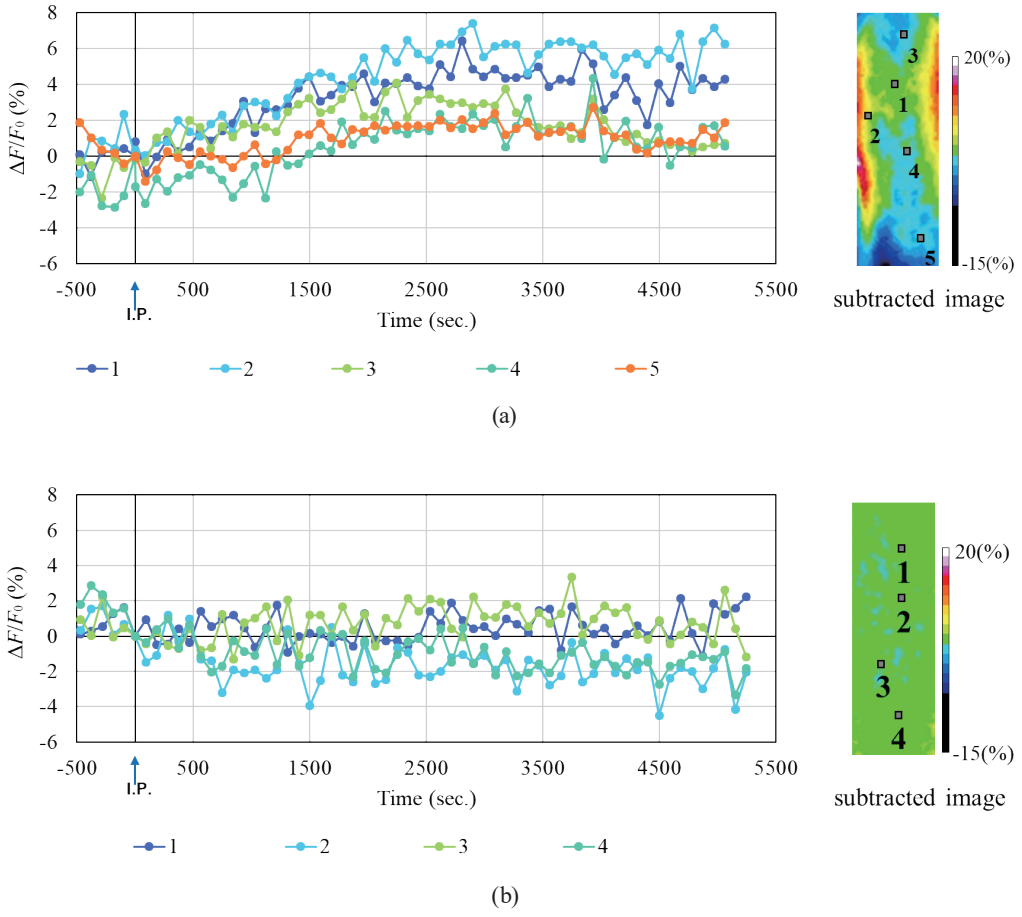

Fig. 8 (Color online) Changes in fluorescence intensity ratio in fluorescence imaging during (a) nicotine administration and (b) PBS administration.

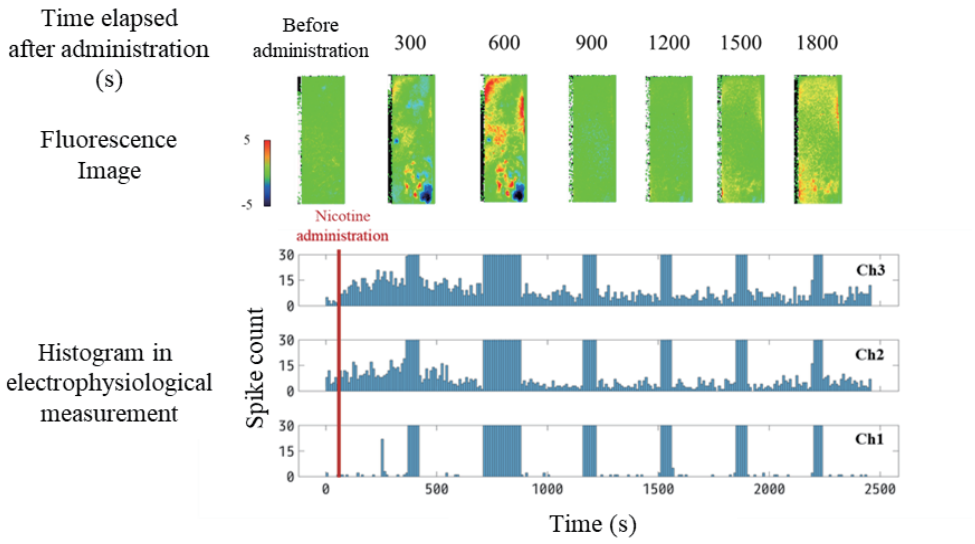

Fig. 9. (Color online) Results of simultaneous electrophysiological measurements and fluorescence imaging in mouse VTA.

size of the histogram is 10 s. In the fluorescence imaging experiment, the peak fluorescence intensity was observed approximately 10 min after nicotine administration. In the electrophysiological measurements, the firing frequency started to increase immediately after the nicotine administration and peaked earlier than that in the fluorescence imaging. These neuronal activations are considered to be induced by the nicotine administration. In the device developed in this study, the image sensor and the microelectrode were about 200 μm apart. The implantation sites of the microelectrodes were $AP = -3.6$ mm and the imaging area was $AP = -3.1$–-3.4 mm in the VTA. Therefore, it can be considered that the results were obtained from neurons with similar activities. In addition, the rapidly increasing spikes in the histogram were caused by the digital signal noise generated by driving the image sensor to the recording microelectrode, which was falsely detected as a spike.

In this study, we identified the source of noise generated during imaging, which is possible to eliminate in the future. Therefore, these results suggest that the multifunctional implantable device developed in this study has potential applications in simultaneous electrophysiological measurements and fluorescence imaging using a CMOS image sensor in a single experiment.

Figure 10 shows the results of the immunohistochemical staining in the VTA. Immunostaining images corresponding to the areas enclosed in dashed lines in the bright-field image on the left panel of Fig. 10 are shown in the center and right panels. The fluorescence images showing the immunostaining of c-Fos were overlaid with TH and VGAT staining images. In Fig. 10(b), brain slices with PBS administered were used, but there was little overlap of staining by the antibodies, indicating that both dopaminergic and GABAergic neurons were not activated by PBS in the VTA. In contrast, the nicotine-stimulated immunostaining results in Fig. 10(a) show that the dopaminergic neurons were activated in the paranigral nucleus (PN) region, whereas the GABAergic neurons were activated in both the parabrachial pigmented area (PBP) and the PN region. In addition, the activation of GABAergic neurons was observed in the PBP region.

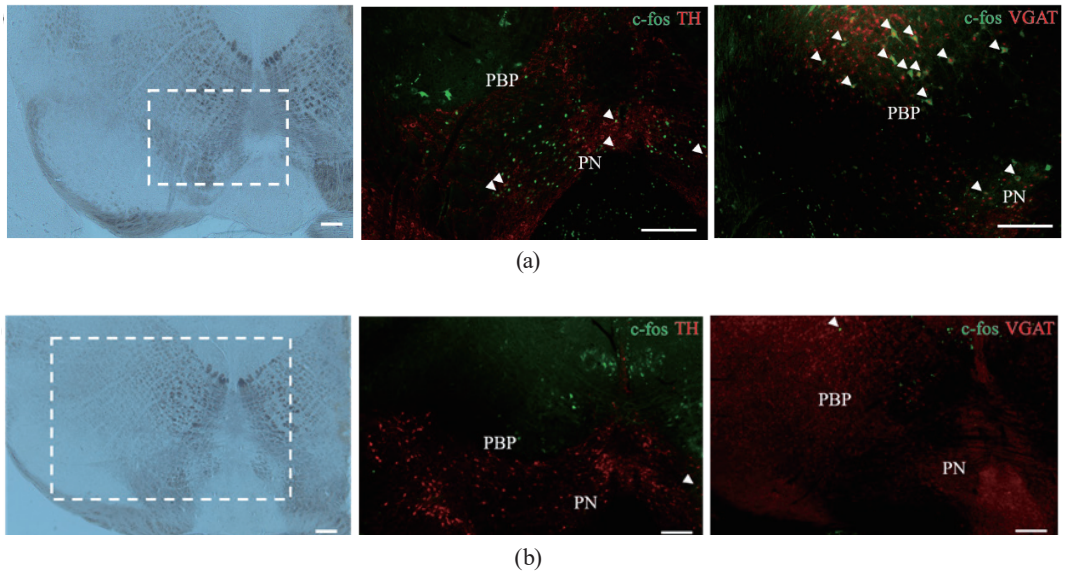

Fig. 10. (Color online) Images showing immunostaining in VTA: (left to right) bright-field images, immunostaining images overlaid with c-Fos (green) and TH (red), and immunostaining images overlaid with c-Fos (green) and VGAT (red). Arrowheads indicate neurons that were stained with both c-Fos and TH/VGAT. (a) Image taken from a brain slice after nicotine administration (0.25 mg/kg). (b) Image taken from a brain slice after PBS administration. All scale bars are 200 μm.

The upregulation of the activity of GABAergic neurons detected by immunostaining is consistent with that detected by the microelectrodes. Dopaminergic neurons are inhibited by GABAergic neurons in the VTA. The discrepancy between the electrophysiological signal peak and the imaging fluorescence intensity peak suggests that the activity of the dopaminergic neurons may increase with time as the inhibition of GABAergic neurons weakens. This needs to be analyzed in detail after the noise in the electrophysiological measurements generated during the imaging operation can be suppressed in the future. The results of this immunostaining strongly suggest that the neuronal activation detected in this study was stimulated by nicotine.

4. Conclusions

In this study, we independently developed microelectrode array and fluorescence imaging devices and evaluated their performance and functions. By integrating each device with epoxy resin, we developed a multifunctional implantable device that allows simultaneous electrophysiological measurements and fluorescence imaging. This is made possible by using a CMOS image sensor, which is unprecedented. Results of *in vivo* experiments using the device we developed showed changes in the fluorescence intensity of neurons synchronized with the spike waveform induced by nicotine administration. Thus, we demonstrated the superiority of the device architecture developed. In the future, neuron-specific measurements by introducing genes such as DAT-Cre can reveal the mechanism of brain neuronal activity in greater detail.

Acknowledgments

This work was supported by JST CREST (JPMJCR1651) and JSPS KAKENHI (JP18H03780). It was also supported through the activities of VDEC, The University of Tokyo, in collaboration with Cadence Design Systems.

References

1 S. Weisenburger and A. Vaziri: Annu. Rev. Neurosci. **41** (2018) 431. https://doi.org/10.1146/annurev-neuro-072116-031458
2 K. K. Ghosh, L. D. Burns, E. D. Cocker, A. Nimmerjahn, Y. Ziv, A. E. Gamal, and M. J. Schnitzer: Nat. Methods **8** (2011) 871. https://doi.org/10.1038/nmeth.1694
3 S. Zhang, Y. Song, M. Wang, Z. Zhang, X. Fan, X. Song, P. Zhuang, F. Yue, P. Chan, and X. Cai: Biosens. Bioelectron. **85** (2016) 53. https://doi.org/10.1016/j.bios.2016.04.087
4 J. Ohta, Y. Ohta, H. Takehara, T. Noda, K. Sasagawa, T. Tokuda, M. Haruta, T. Kobayashi, Y. M. Akay, and M. Akay: Proc. IEEE **105** (2017) 158. https://doi.org/10.1109/JPROC.2016.2585585
5 Y. Sunaga, H. Yamaura, M. Haruta, T. Yamaguchi, M. Motoyama, Y. Ohta, H. Takehara, T. Noda, K. Sasagawa, T. Tokuda, Y. Yoshimura, and J. Ohta: Jpn. J. Appl. Phys. **55** (2016) 03DF02. https://doi.org/10.7567/JJAP.55.03DF02
6 H. Takehara, Y. Ohta, M. Motoyama, M. Haruta, M. Nagasaki, H. Takehara, T. Noda, K. Sasagawa, T. Tokuda, and J. Ohta: Biomed. Opt. Express **6** (2015) 1553. https://doi.org/10.1364/boe.6.001553
7 Y. Sunaga, Y. Ohta, Y. M. Akay, J. Ohta, and M. Akay: IEEE Access **8** (2020) 68013. https://doi.org/10.1109/ACCESS.2020.2985705
8 B. Schilström, N. Rawal, M. Mameli-Engvall, G. G. Nomikos, and T. H. Svensson: Int. J. Neuropsychopharmacol. **6** (2003) 1. https://doi.org/10.1017/S1461145702003188
9 R. Zhao-Shea, L. Liu, L. G. Soll, M. R. Improgo, E. E. Meyers, J. M. Mclntosh, S. R. Grady, M. J. Marks, P. D. Gardner, and A. R. Tapper: Neuropsychopharmacology **36** (2011) 1021. https://doi.org/10.1038/npp.2010.240
10 K. A. Ludwig, N. B. Langhals, M. D. Joseph, S. M. Richardson-Burns, J. L. Hendricks, and D. R. Kipke: J. Neural Eng. **8** (2011) 014001. https://doi.org/10.1088/1741-2560/8/1/014001
11 E. W. Keefer, B. R. Botterman, M. I. Romero, A. F. Rossi, and G. W. Gross: Nat. Nanotechnol. **3** (2008) 434. https://doi.org/10.1038/nnano.2008.174
12 K. Hara and R. A. Harris: Anesth. Analg. **94** (2002) 313. https://doi.org/10.1213/00000539-200202000-00015
13 Immunofluorescence Protocol: Free Floating Section. https://www.creative-diagnostics.com/immunofluorescence-protocol-free-floating-section.htm (accessed January 2022).
14 J. P. Neto, P. Baião, C. Lopes, J. Frazão, J. Nogueira, E. Fortunato, P. Barquinha, and A. R. Kampff: bioRxiv (2018). https://doi.org/10.1101/270058
15 R. Lashgari, X. Li, Y. Chen, J. Kremkow, Y. Bereshpolova, H. A. Swadlow, and J. Alonso: J. Neurosci. **32** (2012) 11396. https://doi.org/10.1523/JNEUROSCI.0429-12.2012

About the Authors

Kyosuke Naganuma received his B.E. degree from the National Institute of Technology, Niihama College, Japan, in 2017 and his M.E. degree from the Nara Institute of Science and Technology (NAIST), Japan, in 2019. He is currently pursuing his Ph.D. degree at NAIST. His research interests include implantable devices, electrophysiology, and neuroscience.

Yasumi Ohta received her B.S. degree in physics from Nara Women's University in 1984. She enrolled in the Faculty of Science at Kyoto University in 2004 and skipped to the master's program at the Graduate School of Science at Kyoto University in 2006. She received her M.S. and Ph.D. degrees in Biophysics from Kyoto University, Kyoto, Japan, in 2008 and 2011, respectively. From 1984 to 1986, she worked at Mitsubishi Electric Corp., Hyogo, Japan. In 2011, she joined the Nara Institute of Science and Technology (NAIST), Nara, Japan, as a postdoctoral fellow. Her research interests include implantable bioimaging CMOS sensors and neuroscience.

Takaaki E. Murakami received his B.E. degree in Electrical and Electronic Engineering from Kindai University, Osaka, Japan, in 2020. He is currently pursuing his M.E. degree at the Nara Institute of Science and Technology (NAIST), Nara, Japan.

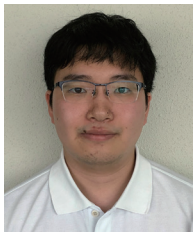

Ryoma Okada received his B.E. degree in Electrical and Electronic Engineering from Shizuoka University, Shizuoka, Japan. He is currently pursuing his M.E. degree at the Nara Institute of Science and Technology (NAIST), Nara, Japan. His research interests include CMOS image sensors for polarization analysis.

Mark Christian Guinto received his B.S. degrees in Chemistry and Materials Engineering from Ateneo de Manila University, Philippines, in 2016 and 2017, respectively. He is currently working toward his Ph.D. degree at the Nara Institute of Science and Technology (NAIST), Nara, Japan, where he also received his M.E. degree in 2019. His research interests include hemodynamic and fluorescence imaging and neurophysiology.

Hironari Takehara received his B.E. and M.E. degrees in Applied Chemistry from Kansai University, Osaka, Japan, in 1984 and 1986, respectively, and his Ph.D. degree in Materials Science from Nara Institute of Science and Technology (NAIST), Nara, Japan in 2015. From 1986 to 2012, he was a semiconductor process engineer at Panasonic Corporation, Kyoto, Japan, where he developed BiCMOS, high-voltage SOI, and optoelectronic IC processes. In 2015, he joined NAIST as a postdoctoral fellow and became an assistant professor in 2019. His current research interests include CMOS image sensors and bioimaging.

Makito Haruta received his B.E. degree in Bioscience and Biotechnology from Okayama University, Okayama, Japan, in 2009, and his M.S. degree in Biological Science and Dr. Eng. degree in Material Science from the Nara Institute of Science and Technology (NAIST), Nara, Japan, in 2011 and 2014, respectively. He was a postdoctoral fellow at NAIST from 2014 to 2016. He joined the Institute for Research Initiatives, NAIST, in 2016, as an assistant professor. In 2019, he joined the Graduate School of Science and Technology, NAIST, as an assistant professor. His research interests include brain imaging devices for understanding brain functions related to animal behavior.

Hiroyuki Tashiro received his B.E. and M.E. degrees in Electrical and Electronic Engineering from Toyohashi University of Technology (TUT), Aichi, Japan, in 1994 and 1996, respectively. He received his Ph.D. degree from Nara Institute of Science and Technology (NAIST), Nara, Japan, in 2017. In 1998, he joined Nidek Co., Ltd., Aichi, Japan, where he worked on the research and development of ophthalmic surgical systems and retinal prostheses. In 2004, he became an assistant professor in the Faculty of Medical Sciences, Kyushu University, Fukuoka, Japan. Since 2019, he has been an associate professor at NAIST. His current research interests include artificial vision systems and neural interfaces.

Kiyotaka Sasagawa received his B.S. degree from Kyoto University, Kyoto, Japan, in 1999, and M.E. and Ph.D. degrees in Materials Science from the Nara Institute of Science and Technology (NAIST), Nara, Japan, in 2001 and 2004, respectively. From 2004 to 2008, he was a researcher at the National Institute of Information and Communications Technology, Tokyo, Japan. In 2008, he joined NAIST as an assistant professor, where he has been an associate professor since 2019. His research interests include bioimaging, biosensing, and electromagnetic field imaging.

Yoshinori Sunaga received his B.E. degree from Chiba University, Japan, in 2012 and M.E. and Ph.D. degrees from the Graduate School of Materials Science, Nara Institute of Science and Technology (NAIST), Japan, in 2014 and 2017, respectively. In 2017, he joined NAIST as a postdoctoral fellow and started a collaboration between NAIST and the University of Houston. In 2019, he joined the University of Houston as a postdoctoral fellow. He is interested in the development of novel devices for observing and accessing the brain activity of animals to reveal new brain mechanisms.

Yasemin M. Akay received her B.S. degree in pharmaceutical sciences from Hacettepe University, Ankara, Turkey, in 1980, and M.S. and Ph.D. degrees in biomedical engineering from Rutgers University, Piscataway, NJ, USA, in 1991 and 1998, respectively. She was a Postdoctoral Fellow with the Physiology and Pharmacology Departments, Dartmouth Medical School and with the Department of Physiology and Biophysics, Boston University, School of Medicine. She is currently an Instructional Associate Professor with the Department of Biomedical Engineering, Cullen College of Engineering, University of Houston, Houston, TX, USA. Her current research interests include molecular neuroengineering, neural growth, and neurodegeneration. She is an Associate Editor for the IEEE Open Journal of Engineering in Medicine and Biology of the IEEE Engineering in Medicine and Biology Society and the IJMS.

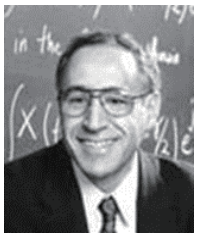

Metin Akay received his B.S. and M.S. degrees in electrical engineering from Bogazici University, Istanbul, Turkey, in 1981 and 1984, respectively, and Ph.D. degree from Rutgers University, Piscataway, NJ, USA, in 1990. He is currently the Founding Chair of the Department of Biomedical Engineering, University of Houston. He is also the President of the IEEE EMBS. He was the Founding Chair of the Annual International Summer School on BIO-X sponsored by the National Science Foundation (NSF) and technically co-sponsored by the IEEE EMBS, and of the Satellite Conference on Emerging Technologies in Biomedical Engineering. He was the Founding Chair of the International IEEE Conference on Neural Engineering in 2003. His current research interests include the investigation of nicotine and alcohol addiction at the molecular, cellular, and system levels during maturation and the development of brain chips for precision medicine.

Jun Ohta received his B.E., M.E., and Dr. Eng. degrees in Applied Physics from The University of Tokyo, Japan, in 1981, 1983, and 1992, respectively. In 1983, he joined Mitsubishi Electric Corporation, Hyogo, Japan. From 1992 to 1993, he was a visiting scientist at the Optoelectronics Computing Systems Center, University of Colorado Boulder. In 1998, he joined the Graduate School of Materials Science, Nara Institute of Science and Technology (NAIST), Nara, Japan, as an associate professor. He was appointed as a professor in 2004. His current research interests include smart CMOS image sensors for biomedical applications and retinal prosthetic devices. He is a fellow of IEEE, the Japan Society of Applied Physics, and the Institute of Image, Information, and Television Engineers. He serves as an editor of Sensors and Materials and an associate editor of IEEE Transactions on Biomedical Circuits and Systems and is on the editorial board of the Journal of Engineering, IET.